Diffuse Electron Scattering in β-Phase Alloys

K. OTSUKA, C. M. WAYMAN, AND H. KUBO

Nonradial diffuse streaks and complex diffuse scattering patterns occurring in β-phase Cu-Al-Ni(DO_3) and Cu-Zn(B_2) alloys have been systematically studied in detail using transmission electron diffraction. As a consequence, the presence of intense $\langle 110\rangle^*_\beta$ rel rods has been confirmed unambiguously, in addition to weak $\{111\}^*_\beta$ rel walls arising from the Honjo effect. It was found that all the complex diffuse patterns could be explained on the basis of the intersections of the observed rel rods with the Ewald sphere. From the direction of the rel rods and conditions for their extinction it is concluded that they originate from the presence of a low frequency transverse acoustic phonon mode, $\langle 110\rangle^*\langle \bar{1}10\rangle$. Since identical results were obtained for both the Cu-Al-Ni and Cu-Zn alloys it appears that such effects may be generally characteristic of ordered β-phase alloys. The relation between the diffuse rel rods and the known martensitic transformations in these alloys is also considered.

I. INTRODUCTION

SINCE the breakdown of the classical theory of nucleation,[1] the nucleation mechanism in martensitic transformations has for sometime remained an important unsolved problem. Various alternative attempts have been made, both experimentally and theoretically, and investigators are now paying some attention to the possible role of lattice vibrations,[2,3] and the presence of defects such as dislocations, stacking faults and boundaries as means to overcome the nucleation difficulty.[4,5] Experimentally, the lattice vibration effects can be studied by measuring elastic constants (*e.g.*, the ultransonic technique), by measuring phonon dispersion curves by inelastic neutron scattering, or by electron and X-ray diffraction techniques. In the particular case of β-phase alloys extensive studies have shown considerable lattice softening in $C' = [C_{11} - C_{12}]/2$ (Ref. 6) or low values of C' (in the case where the temperature dependence is small)[7] prevail over a wide temperature range prior to a martensitic transformation, as originally suggested by Zener.[8] Anomalies are also found in electron diffraction and microscopy. That is, the diffraction patterns from these alloys are considerably more complex than those from a simple ordered bcc structure of the DO_3 or B_2 types.[9,10] Such patterns usually contain "extra" reflections, which are often ascribed to an ω-phase[11] or to 2H type reflections[12] (or others), and streaks in various directions.[13] Some authors claim that these effects are "premonitory", prior to a subsequent martensitic transformation,[14,15] while others believe that they result from decomposition processes which have nothing to do with the martensitic transformation since the β-phase alloys generally decompose into several phases and even rapid quenching cannot suppress decomposition completely.[9] A distinction between the above two interpretations is not very clear at present. This chaotic situation exists because various phenomena occur concurrently in these materials which makes it difficult to understand each separate phenomenon in a straightforward way. In view of these circumstances the present authors have carried out an extensive study of diffraction phenomena in the matrix phase of two β-phase alloys.

Since the matrix phase in β-phase alloys generally has either the DO_3 or B_2 type structure, we chose two alloys, Cu-Al-Ni(DO_3) and Cu-Zn(B_2) as representative of β-phase alloys. From electron microscopy and diffraction of these alloys, we observed the presence of an ω-phase, a 2H-type phase, and diffuse streaks and diffuse patterns. However, we treat only the diffuse diffraction in the present paper since these effects have been analyzed both consistently and systematically. Thus, the purpose of the present paper is to clarify the nature and origin of the diffuse streaks and diffuse patterns in these alloys.

II. EXPERIMENTAL PROCEDURE

The Cu-Al-Ni alloy was prepared from 99.99 pct Cu, 99.99 pct Al and 99.9 pct Ni by melting in a high frequency vacuum furnace, followed by casting into a water-cooled copper mold. The resulting ingot was homogenized at 1000°C for 24 h and then chemically analyzed. The results of the analysis showed the composition to be Cu-14.2Al-4.3Ni (wt pct). After homogenization the ingot was hot forged at 900 to 950°C, and then hot rolled at the same temperature to a thickness of 0.7 mm. Specimens were then solution treated at 1000°C for 1 h followed by a water quench. The resulting M_s temperature was about 0°C. Finally, specimens were electropolished to electron transparency at room temperature in a solution of H_3PO_4 saturated with CrO_3.

A Cu-39.6 wt pct Zn alloy, with M_s temperature about − 50°C, was prepared from 99.99 pct Cu and 99.999 pct Zn by melting in an evacuated quartz tube, following which single crystal rods 7 mm in diam were grown using the Bridgman technique and an argon atmosphere. Discs with [100], [110] and [111] orientations were cut from the crystal rods with a slow-speed diamond cutter, and then shaped into

K. OTSUKA is with the Institute of Scientific and Industrial Research, Osaka University, Osaka, Japan, and C. M. WAYMAN and H. KUBO are with the Department of Metallurgy and Mining Engineering, and the Materials Research Laboratory, University of Illinois at Urbana-Champaign, Urbana, IL 61801.

Manuscript submitted January 9, 1978.

ISSN 0360-2133/78/0810-1075$00.75/0

specimens 3 mm in diam and 0.5 mm in thickness by electropolishing in an H_3PO_4-CrO_3 solution. These specimens were then placed in evacuated quartz tubes and solution treated for 5 min at 850°C, following which the quartz tubes were quenched (and immediately broken) in a 10 pct NaOH solution at −15°C. The specimens were then lightly mechanically polished, followed by electrolytic jet polishing in $H_3PO_4/C_2H_5OH/H_2O$ (1 : 3 : 36), and finish-polished in a HNO_3/CH_3OH solution (1 : 3) at −45°C. Electron microscopy was performed at room temperature unless otherwise specified.

III. RESULTS

Figures 1 and 2 show a series of electron diffraction patterns taken from the Cu-Al-Ni and Cu-Zn alloys, respectively. The patterns, from different specimens in order to cover a tilting range of 90 deg, are arranged to show the changes during tilting around the $[110]^*_\beta$ axis* from a $[001]_\beta$ orientation to a $[\bar{1}10]_\beta$ orientation. From these figures, three different diffraction phenomena are observed, in addition to the fundamental and superlattice reflections from the β matrix phase.

*The asterisk represents a quantity in reciprocal space. Thus, *e.g.*, $[uvw]^*$ and $(hkl)^*$ are directions and planes, respectively, in reciprocal space.

i) Streaks (Figs. 1 and 2(*a*, *b*, *c*, *e*, *f*, *g*, *h*, *i*, and *j*)); most of the streaks run along $\langle 110\rangle^*_\beta$ directions, but some appear along $\langle 1\bar{3}2\rangle^*_\beta$ (*f*) and $\langle 11\bar{2}\rangle^*_\beta$ (*j*).

ii) Diffuse patterns (Figs. 1 and 2(*b*, *c*, *d*, *e*, *f*, *h*, *i* and *j*)); as indicated by arrows, these reflections usually appear in a very diffuse and weak manner. The shapes of the reflections are different from one orientation to another, and their configurations are sometimes quite complex at first sight as shown in (*f*) and (*i*). Extra reflections in (*b*) and (*h*) are of the same

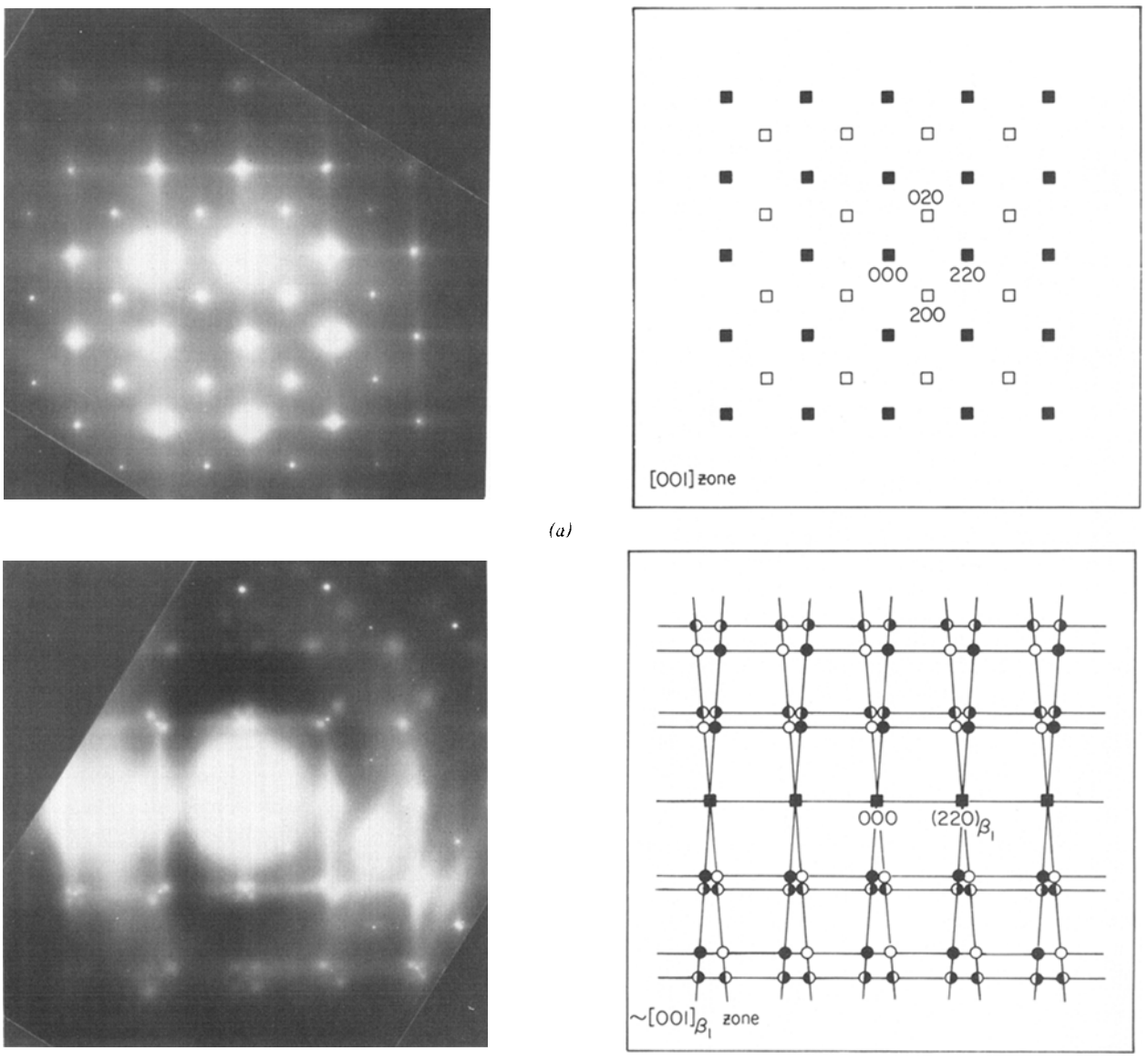

Fig. 1—Changes in the electron diffraction patterns for a Cu-Al-Ni alloy during rotation around the $[110]^*_\beta$ axis. The angle of rotation, α, from the $[001]^*_\beta$ orientation is: (*a*) 0 deg, (*b*) ≃0 deg, (*c*) 15.8 deg, (*d*) 19.5 deg, (*e*) 25.2 deg, (*f*) 35.3 deg, (*g*) 54.7 deg, (*h*) ≃55 deg, (*i*) 70.5 deg and (*j*) 90 deg. Arrows indicate diffuse patterns. See text for the meaning of symbols used in the index diagrams.

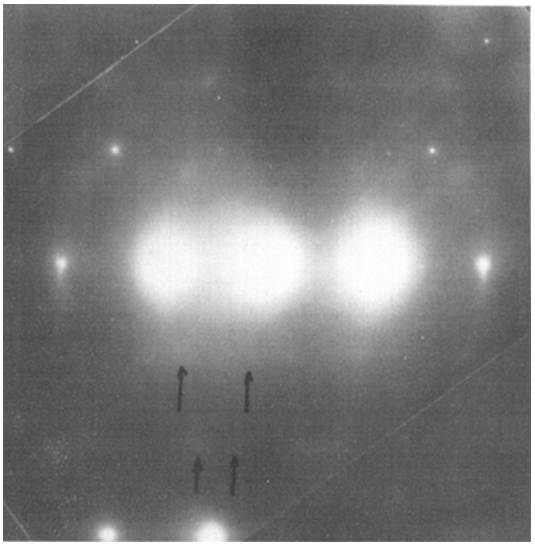

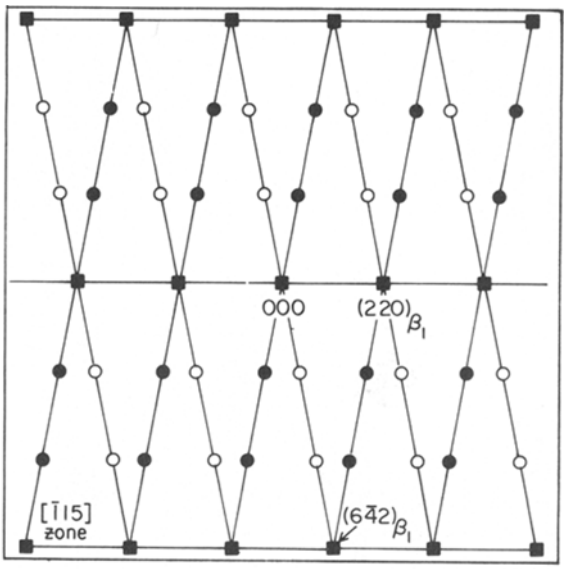

(c)

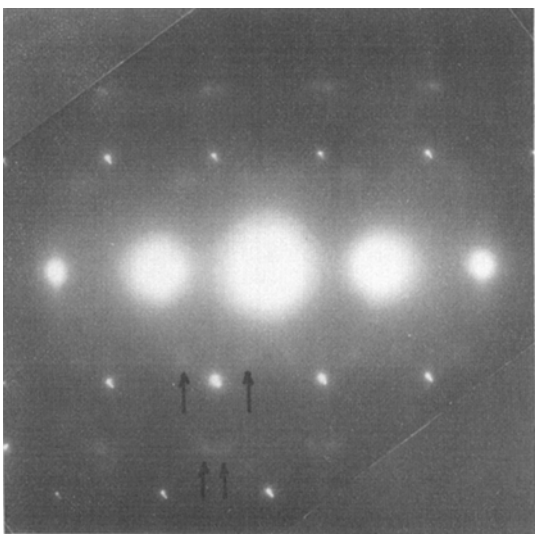

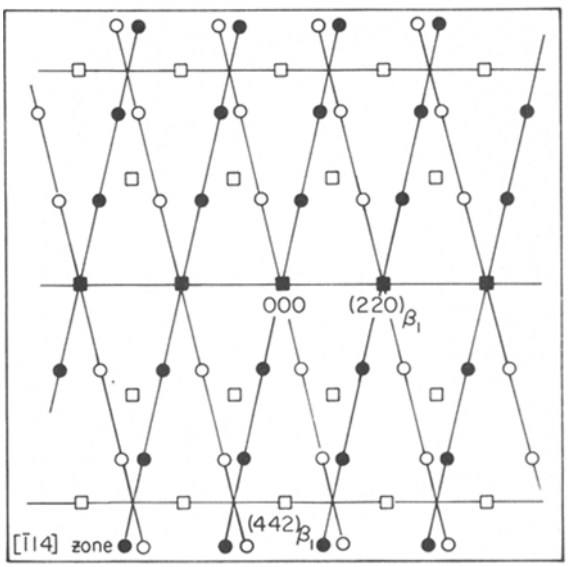

(d)

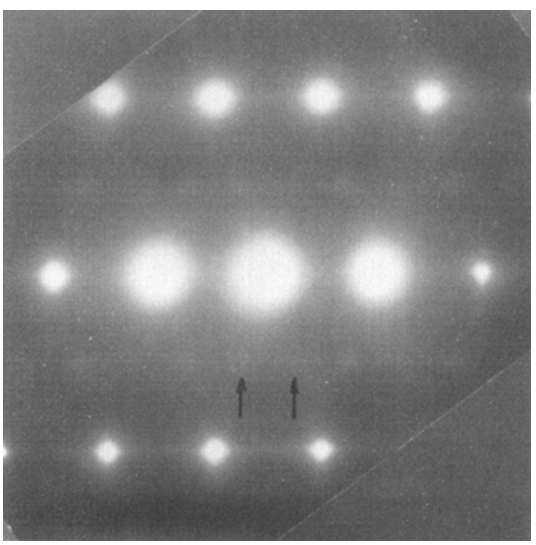

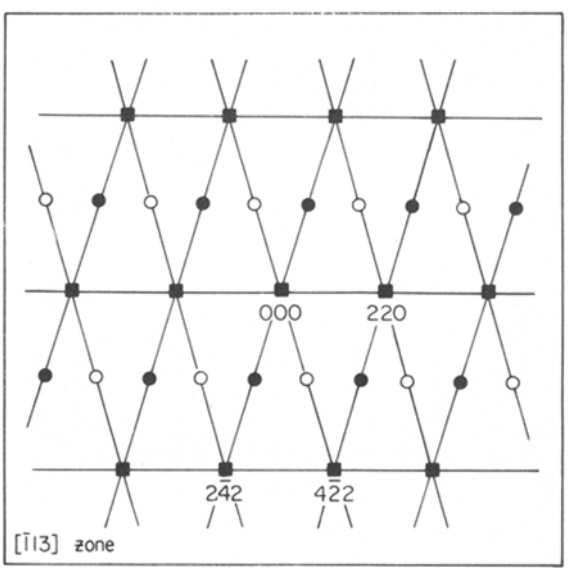

(e)

Fig. 1—Continued.

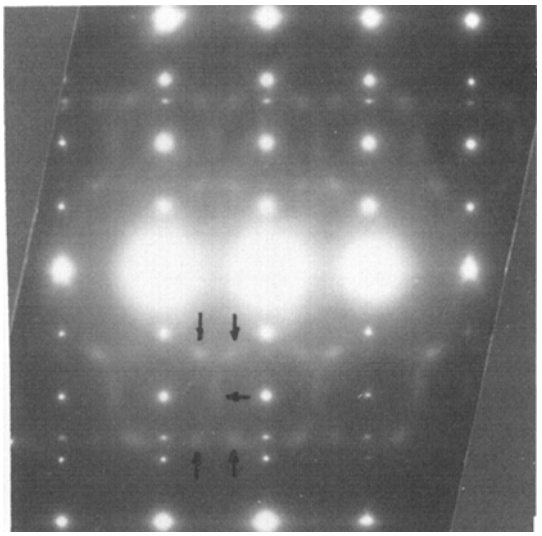

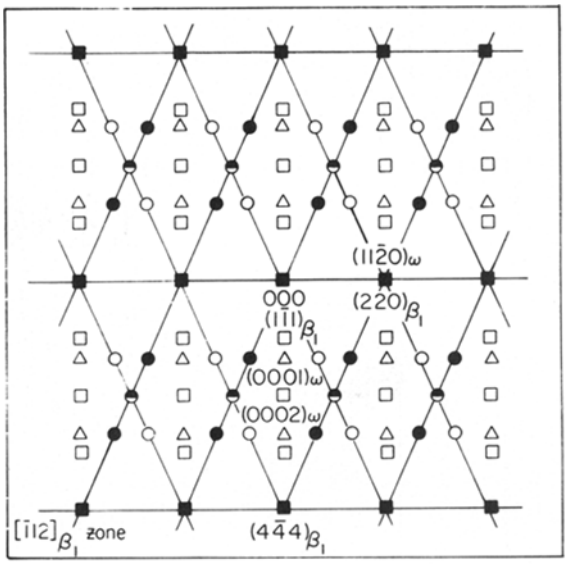

(f)

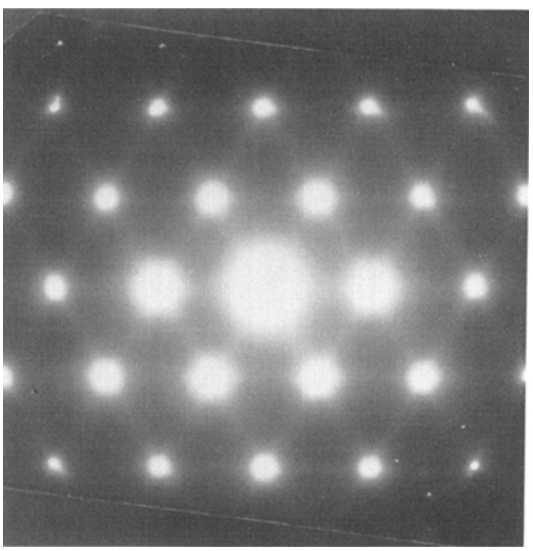

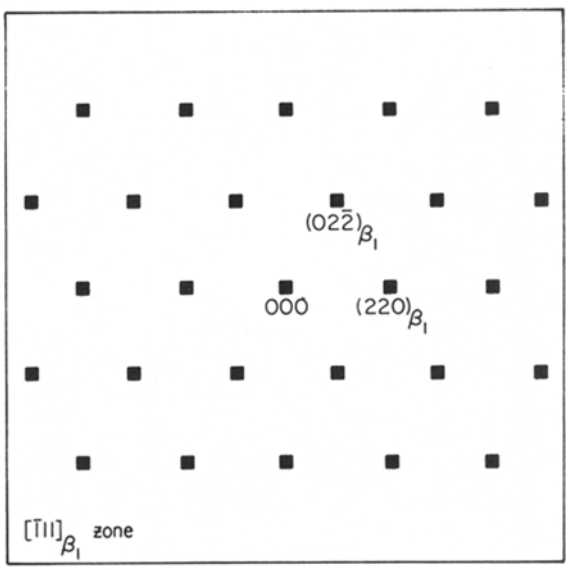

(g)

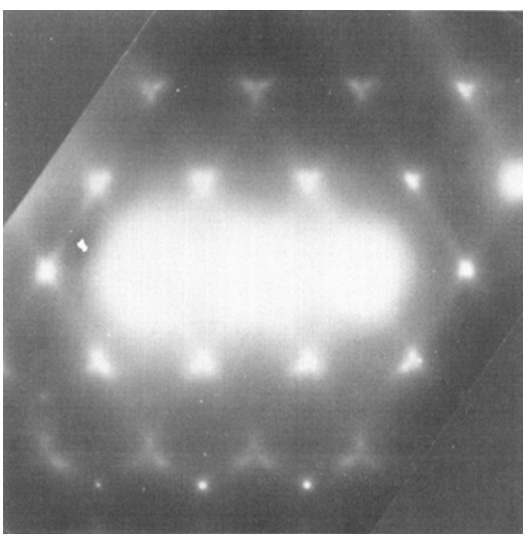

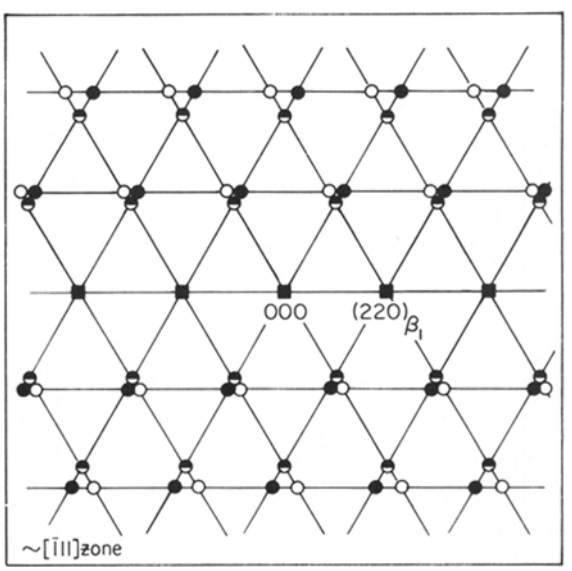

(h)

Fig. 1–Continued.

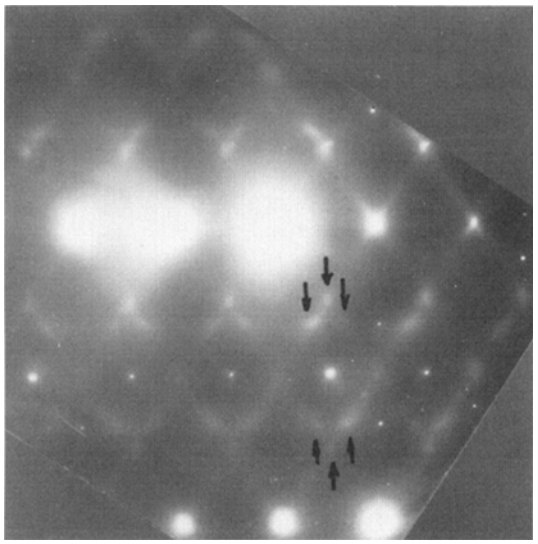

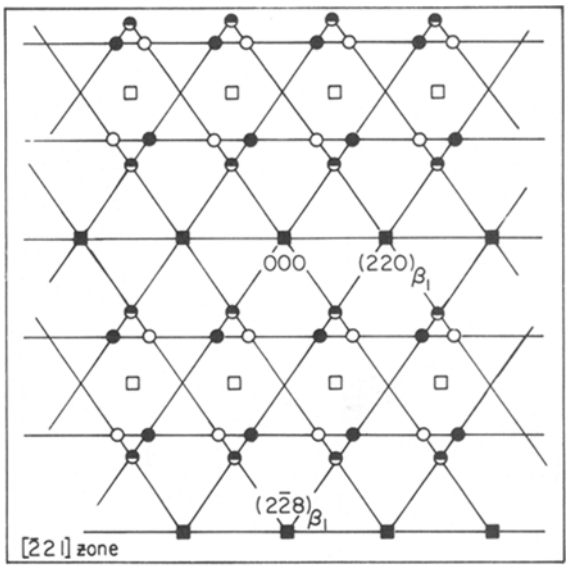

(i)

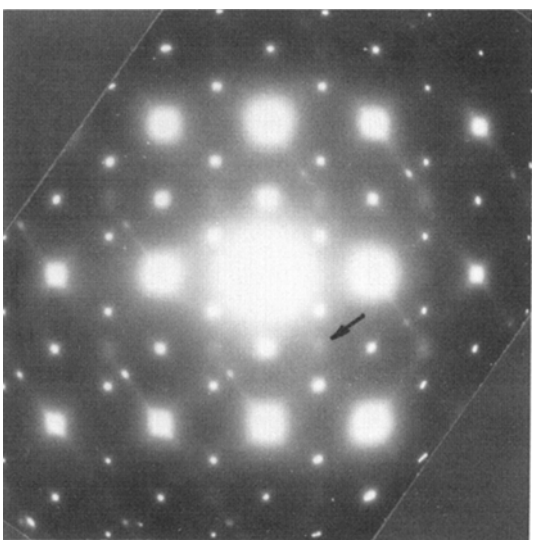

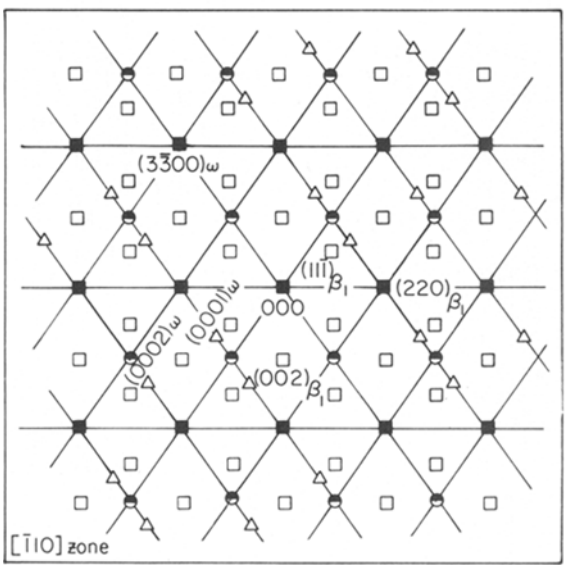

(j)

Fig. 1—Continued.

type, as will be shown later. (The extra reflections in Figs. 1(*h*) and 2(*h*) appear at different locations because the tilt angle is opposite in sense with respect to the $(111)^*_\beta$ plane lying between them.)

iii) ω-phase (Figs. 1 and 2(*f* and *j*)); rather weak but sharp reflections are observed in (*f*) and (*j*). These can be consistently indexed as ω-phase reflections (see the associated index diagrams) as reported in Cu-Sn[11] and other β-phase alloys. In addition to the above reflections, 2H type reflections as reported by Takezawa and Sato for a Cu-Zn alloy[12] were observed at times, but neither the 2H type nor the ω-phase reflections are further described here since they are considered irrelevant to the purposes of the present paper.

Before going into details, the explanation of symbols used in the associated index diagrams of Fig. 1 is given below. Some symbols (used for the diffuse reflections) signify only a literal meaning at present, and a more accurate description for these will be given later. (The index diagrams for the Cu-Zn alloy have been omitted because they are essentially the same as those for the Cu-Al-Ni alloy except for the conditions that the superlattice spots with odd indices in Fig. 1 do not appear in Fig. 2, and that all the indices in Fig. 2 should be divided in half in order to compare them to those in Fig. 1.)

- ■ fundamental reflections of the β matrix phase,
- □ superlattice reflections of the β matrix phase,
- △ ω-phase reflections,
- ● intersections of $[\bar{1}01]^*_\beta$ streaks with the Ewald sphere,
- ○ intersections of $[011]^*_\beta$ streaks with the Ewald sphere,
- ◑ intersections of $[0\bar{1}1]^*_\beta$ streaks with the Ewald sphere,
- ◐ intersections of $[101]^*_\beta$ streaks with the Ewald sphere, and
- ◓ intersections of $[1\bar{1}0]^*_\beta$ streaks with the Ewald sphere.

We now consider the diffuse streak patterns first. It is widely known that Honjo *et al*[16] reported nonradial streak patterns in electron and X-ray diffraction pat-

terns from a number of metallic and nonmetallic materials. They found that rel walls were present in these materials which run normal to the close-packed directions in real space, and that the observed streaks correspond to the intersections of these rel walls with the Ewald sphere. These investigators further suggested that the rel walls arise as a result of a more or less independent linear chain motion in the close-packed directions, since atoms in a close-packed direction cannot move relative to each other. If we apply this effect to β-phase alloys, we expect the presence of $\{111\}^*_\beta$ rel walls, since the close-packed directions in these alloys are of the type $\langle 111\rangle_\beta$. In fact, all the streaks in Figs. 1 and 2, including those in (*f*) and (*j*), can be explained as intersections of $\{111\}^*_\beta$ rel walls with the Ewald sphere. Thus, the diffuse streak patterns in β-phase alloys are generally accepted as the result of the Honjo effect,[13] although some authors[10,17] claim the presence of $\langle 110\rangle^*_\beta$ rel rods. However, as far as the present authors know, no systematic, clear-cut experiments have been made to distinguish between the two possibilities, *i.e.*, $\{111\}^*_\beta$ walls or $\langle 110\rangle^*_\beta$ streaks *per se*. In fact, the distinction is not a straightforward matter, since $\langle 110\rangle^*_\beta$ rel rods always lie in $\{\bar{1}11\}^*_\beta$ rel walls and the observed $\langle 110\rangle^*_\beta$ streaks can be explained by either model. We can attack this problem as follows.

The above question has been raised, in spite of the fact that all streak patterns in Figs. 1 and 2 can be explained by the presence of $\{111\}^*_\beta$ rel walls as stated above, on the basis of the following observations. First, the $\langle 110\rangle^*_\beta$ streaks are usually much more intense than the other observed streaks such as the $\langle 1\bar{3}2\rangle^*_\beta$ streaks in (*f*) and the $\langle 112\rangle^*_\beta$ streaks in (*j*), both of which can be interpreted as the result of the intersections of $\{111\}^*_\beta$ walls with the Ewald sphere. Secondly, when a specimen is tilted slightly from a perfectly rational orientation, extra reflections appear

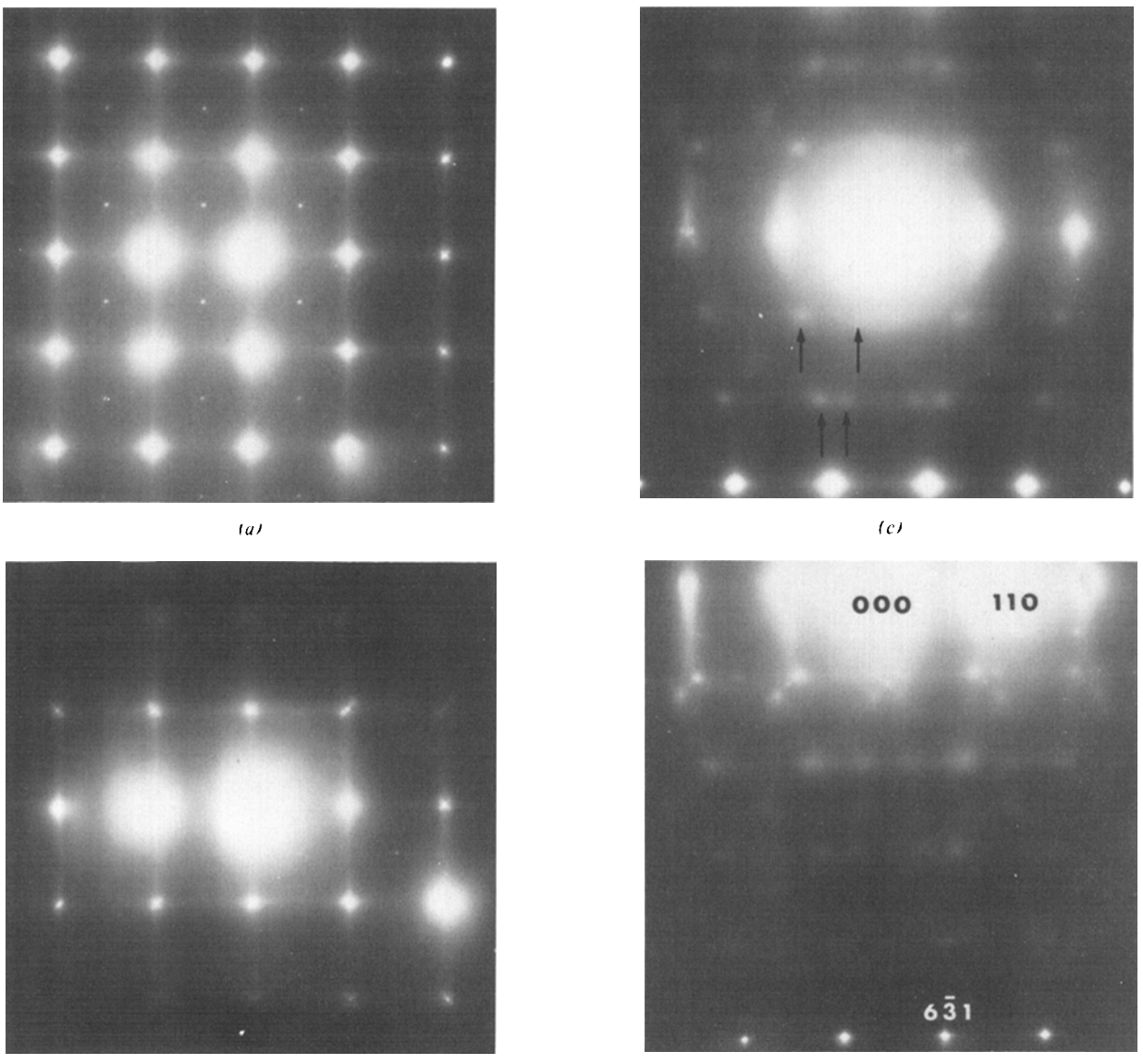

Fig. 2—Changes in the electron diffraction patterns for a Cu-Zn alloy when rotated around the $[110]^*_\beta$ axis. The patterns are essentially the same as those in Fig. 1 except for (*d*) and (*i*) which are different orientations. (*a*) $[001]_\beta$ $\alpha = 0$ deg, (*b*) $\sim[001]_\beta$, (*c*) $[\bar{1}15]_\beta$ $\alpha = 15.8$ deg, (*d*) $[\bar{1}19]_\beta$ $\alpha = 8.9$ deg, (*e*) $[\bar{1}13]_\beta$ $\alpha = 25.2$ deg, (*f*) $[\bar{1}12]_\beta$ $\alpha = 35.3$ deg, (*g*) $[\bar{1}11]_\beta$ $\alpha = 54.7$ deg, (*h*) $\sim[\bar{1}11]_\beta$, (*i*) $\sim[\bar{3}31]_\beta$ $\alpha = 76.9$ deg, and (*j*) $[\bar{1}10]_\beta$ $\alpha = 90$ deg.

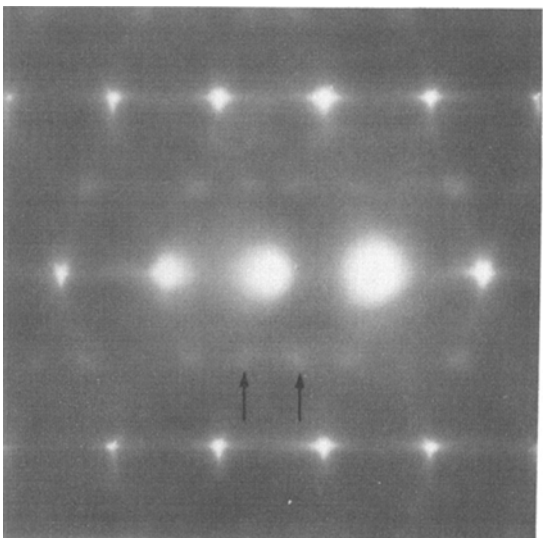

(e)

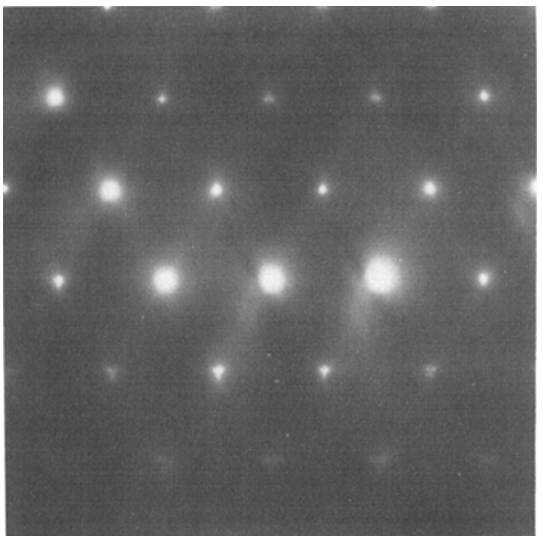

(h)

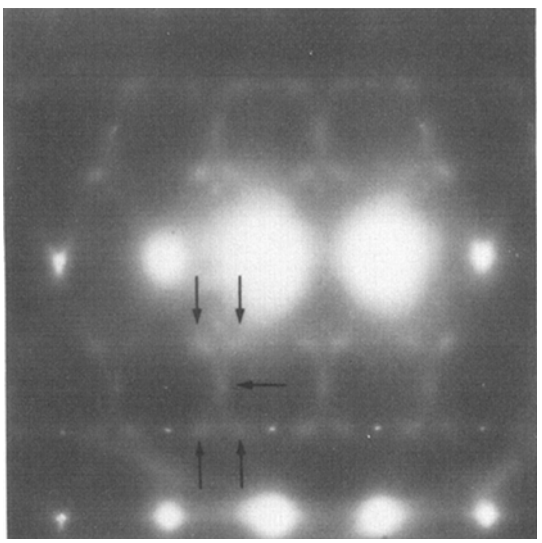

(f)

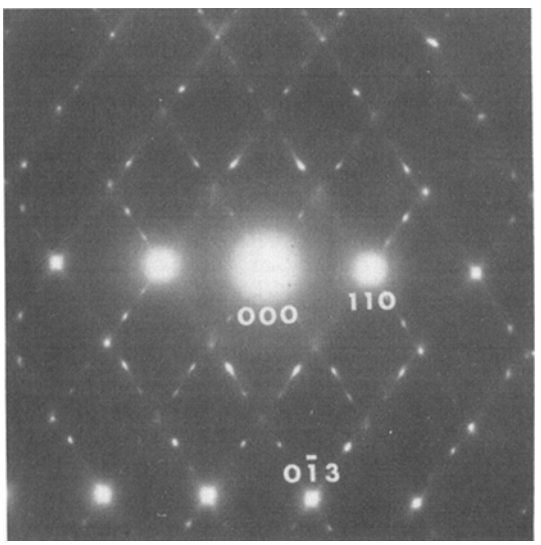

(i)

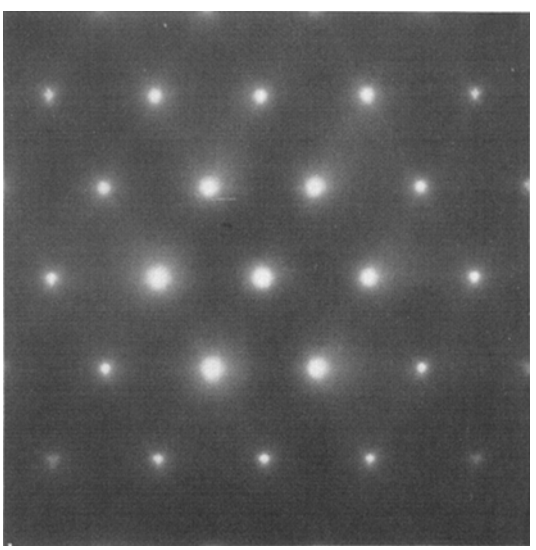

(g)

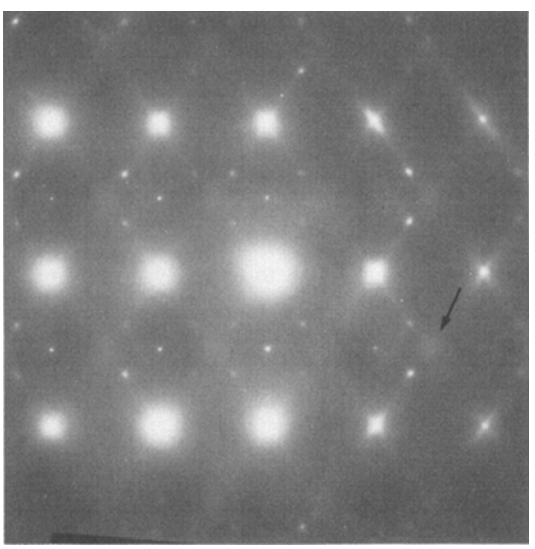

(j)

Fig. 2–Continued.

around each reciprocal lattice point and the separation of the extra reflections becomes wider as they become farther from the tilting axis ((*b*) and (*h*) in Figs. 1 and 2, and (*d*) in Fig. 2). This is a strong indication to show that the extra reflections appear as a result of the intersections of spikes or streaks with the Ewald sphere, as previously demonstrated in an extensive study of epitaxial cobalt films.[18] In fact, the relative position of each extra reflection in (*b*) and (*h*), and (*d*) in Fig. 2 is consistent with what is expected from the presence of $\langle 110\rangle^*_\beta$ rel rods, as indicated in each index diagram. Furthermore, it is to be emphasized that all the complex diffuse patterns in Figs. 1 and 2(*c*, *d*, *e*, *f*, *i* and *j*) can be explained as intersections of these $\langle 110\rangle^*_\beta$ rel rods with the Ewald sphere, as shown in each index diagram and described in detail later. Thus, there are good reasons to believe the presence of $\langle 110\rangle^*_\beta$ rel rods in the Cu-Al-Ni and Cu-Zn alloys, and that the apparent $\langle 110\rangle^*_\beta$ streaks in Figs. 1 and 2 are really $\langle 110\rangle^*_\beta$ rel rods in reciprocal space rather than simple intersections of homogeneous $\{\bar{1}11\}^*_\beta$ rel planes with the Ewald sphere. However, the above considerations do not deny the presence of $\{\bar{1}11\}^*_\beta$ rel walls. We have to note as well that other weak streaks are also present such as $\langle 112\rangle^*_\beta$ streaks in Figs. 1 and 2(*j*) and $\langle 1\bar{3}2\rangle^*_\beta$ streaks in Figs. 1 and 2(*f*). Obviously these are not explained by $\langle 110\rangle^*_\beta$ rel rods but can be explained by the intersections of $\{\bar{1}11\}^*_\beta$ rel walls with the Ewald sphere. Therefore the view adopted here is as follows. In both the Cu-Al-Ni and Cu-Zn alloys, weak $\{\bar{1}11\}^*_\beta$ rel planes are present, which contain more intense $\langle 110\rangle^*_\beta$ rel rods.

Although we have been led to conclude the presence of $\langle 110\rangle^*_\beta$ rel rods above, more detailed study is required for internal consistency. Careful observations of Figs. 1 and 2 reveal the following as characteristic of the $\langle 110\rangle^*_\beta$ streaks.

i) $\langle 110\rangle^*$ streaks are usually observed only along lines which connect fundamental reflections. The case of Fig. 1(*a*) is the only exception, where faint $\langle 110\rangle^*_\beta$ streaks are observed even along lines which connect superlattice reflections, but their intensity is extremely weak.

ii) The $\langle 110\rangle^*_\beta$ streaks are absent on the $\langle 110\rangle^*_\beta$ directions which pass through the origin. In Figs. 1 and 2(*a*) and (*g*), $\langle 110\rangle^*_\beta$ streaks are observed, even on directions which go through the origin. But, these are the result of double diffraction, as may be seen by comparing (*a*) and (*b*), and (*g*) and (*h*) respectively. In (*b*) and (*h*), the specimens are slightly tilted around the $[110]^*_\beta$ axis so as to suppress the fundamental source reflections which cause $\langle 110\rangle^*_\beta$ streaks through the origin by double diffraction.

iii) There appears to be an extinction rule for the appearance of $\langle 110\rangle^*_\beta$ streaks. For example, $[110]^*_\beta$ streaks are absent in the $[\bar{1}10]_\beta$ orientation (*j*) and the $[\bar{2}21]_\beta$ orientation (*i*), Fig. 1, and in the $[\bar{3}31]_\beta$ orientation, Fig. 2(*i*) although fundamental reflections along the $[110]^*_\beta$ direction appear in these orientations.

We now look for the origin of the $\langle 110\rangle^*_\beta$ streaks, consistent with the above characteristics. Based on the facts that $\langle 110\rangle^*_\beta$ rel rods lie in $\{\bar{1}11\}^*_\beta$ rel walls, and that a dark field image using these diffuse streaks does not reveal any contrast, we consider phonon scattering. Phonon scattering was previously used by Chandra and Purdy[19] to explain the so-called "1/3 reflections" in Ti-Ni, and later by Hehemann *et al*[20,21] for the same purpose in Ti-Ni and Au-Cd. We follow a similar treatment, with some modification, in the following.

We consider a displacement wave of the form

$$\mathbf{R}_n = A(q)\boldsymbol{\epsilon}_0 \cos 2\pi\,(\mathbf{q}\cdot\mathbf{r}_n - \nu t) \qquad [1]$$

where

$\mathbf{R}_n$ = displacement vector,
$A(q)$ = displacement wave amplitude,
$\boldsymbol{\epsilon}_0$ = unit polarization vector,
$\mathbf{q}$ = phonon wave vector,
$\mathbf{r}_n$ = lattice vector,
ν = frequency, and
t = time.

The amplitude of the diffracted wave is then,

$$\phi_g = \sum_n F_g e^{-2\pi i(\mathbf{g}+\mathbf{s})\cdot(\mathbf{r}_n+\mathbf{R}_n)} \qquad [2]$$

where

$\mathbf{g}$ = reciprocal lattice vector,
$\mathbf{s}$ = vector representing the deviation from a reciprocal lattice point (diffraction error), and
F_g = structure factor.

Assuming that $A(q)$ is very small,

$$\phi_g = F_g\sum_n e^{-2\pi i\mathbf{s}\cdot\mathbf{r}_n} - \pi i F_g A(q)\,(\mathbf{g}+\mathbf{s})\cdot\boldsymbol{\epsilon}_0 \times\Big[e^{-2\pi i\nu t}\sum_n e^{-2\pi i(\mathbf{s}-\mathbf{g})\cdot\mathbf{r}_n} + e^{2\pi i\nu t} \times\sum_n e^{-2\pi i(\mathbf{s}+\mathbf{g})\cdot\mathbf{r}_n}\Big]. \qquad [3]$$

The first term in the above represents diffraction from a crystal without displacement, and the second and third terms the effect of phonon scattering. It can be seen from the latter two terms that subsidiary maxima appear at $\mathbf{s} = \pm\mathbf{q}$ due to phonon scattering. Next, the amplitude of the displacement wave is obtained from the results of lattice dynamics as,[22]

$$A^2 = E_\nu/2\pi^2 N m\nu^2 \qquad [4]$$

where

E_ν = phonon energy, $\simeq kT$ when the temperature is not very low,
m = atomic mass (average), and
N = number of atoms in the crystal.

Thus, from Eqs. [3] and [4], the intensity of phonon scattering is

$$|\phi_g^{ph}|^2 \propto \frac{|F_g|^2\cdot|(\mathbf{g}+\mathbf{q})\cdot\boldsymbol{\epsilon}_0|^2}{\nu^2}. \qquad [5]$$

If the displacement wave Eq. [1] is transverse in nature, which will be the present concern, as shown later, then $\mathbf{q}\cdot\boldsymbol{\epsilon}_0 = 0$. Thus

$$|\phi_g^{ph}|^2 \propto \frac{|F_g|^2\cdot|\mathbf{g}\cdot\boldsymbol{\epsilon}_0|^2}{\nu^2}. \qquad [5']$$

When phonons are continuously distributed in $\mathbf{q}$-space such that the directions of the wave vectors and

polarization vectors are unchanged, streaks along the vector $\mathbf{q}$ result from the above scheme, and Eqs. [5] or [5′] still hold at each point along the streaks.

From the above, the characteristics of the $\langle 110\rangle^*_\beta$ streaks described previously are easily rationalized. The first characteristic is considered to begin with. We take 200_β and 220_β for Cu-Al-Ni and 100_β and 110_β for Cu-Zn as representative of superlattice and fundamental reflections, respectively. Then simple calculations show that $|F_{200}|^2/|F_{220}|^2 \simeq 1/50$ for the Cu-Al-Ni alloy, and that $|F_{100}|^2/|F_{110}|^2 \simeq 1/3750$ for the Cu-Zn alloy. Since the intensity of phonon scattering is proportional to $|F_g|^2$, the intensity of the streaks associated with superlattice reflections is much weaker than that of those associated with fundamental reflections. Thus the first characteristic has been rationalized.

The second characteristic can also be rationalized if the displacement wave is transverse in nature. For a streak going through the origin the vectors $\mathbf{g}$ and $\mathbf{q}$ are parallel, while $\mathbf{q}$ and $\boldsymbol{\epsilon}_0$ are normal for a transverse wave. Thus, $\mathbf{g}\cdot\boldsymbol{\epsilon}_0 = 0$, and consequently $|\phi_g^{ph}|^2 = 0$ for Eq. [5′]. Therefore, the second characteristic can be taken as an indication that the $\langle 110\rangle^*_\beta$ streaks in the present case is due to the presence of a transverse phonon mode.

In order to rationalize the third characteristic, we have to assume an operating phonon mode which satisfies the following three conditions. First, it must be a transverse wave as discussed above. Secondly, the phonon wave vector $\mathbf{q}$ must be parallel to $\langle 110\rangle^*_\beta$, since the observed streaks lie along $\langle 110\rangle^*_\beta$. Thirdly, from Eq. [5′], the frequency ν of the phonon must be substantially low over a wide range of the branch of concern. It is known from the work of Hoshino *et al*[23] for the Cu-Al-Ni alloy that phonons with wave vector $\mathbf{q} \parallel \langle 110\rangle^*_\beta$ and polarization vector $\boldsymbol{\epsilon}_0 \parallel \langle \bar{1}10\rangle_\beta$ (TA_2 mode in Ref. 23) satisfies these conditions, and very similar characteristics are also found for the Cu-Zn alloy.[24] If we, therefore, choose this phonon mode, the characteristics listed in the third category are consistently explained as follows.

First we consider the case of the $[\bar{1}10]_\beta$ orientation [Figs. 1 and 2(*j*)]. Since the 220_β reflection lies in this zone, $\mathbf{q}$ must be parallel to $[110]^*_\beta$. Once $\mathbf{q}$ is specified as such, then the polarization vector is uniquely determined as $\boldsymbol{\epsilon}_0 \parallel [\bar{1}10]_\beta$ which is parallel to the zone axis. Thus, $\mathbf{g}\cdot\boldsymbol{\epsilon}_0 = 0$ for any $\mathbf{g}$ vector in this zone. Therefore, $|\phi_g^{ph}|^2 = 0$ and $[110]^*_\beta$ streaks are absent in this zone.

Next to consider is the case of the $[\bar{2}21]_\beta$ orientation in Fig. 1 and the $[\bar{3}31]_\beta$ orientation in Fig. 2. Again, $\mathbf{q} \parallel [110]^*_\beta$ and $\boldsymbol{\epsilon}_0 \parallel [\bar{1}10]_\beta$, but not all $\mathbf{g}$ vectors are perpendicular to $\boldsymbol{\epsilon}_0$ in this case. However the maximum value of $\mathbf{g}\cdot\boldsymbol{\epsilon}_0/|\mathbf{g}|\cdot|\boldsymbol{\epsilon}_0|$ is only 0.236 for the former and 0.229 for the latter. Thus, the $[110]^*_\beta$ streaks are still barely visible. However, as the orientation becomes closer to $[001]_\beta$, $\mathbf{g}\cdot\boldsymbol{\epsilon}_0$ becomes larger and the $[110]^*_\beta$ streaks become visible as shown in Figs. 1 and 2, (*a*) to (*g*). The same argument can be applied to explain why weak $\langle 110\rangle^*_\beta$ streaks are observable even along lines connecting superlattice reflections in the $[001]_\beta$ orientation in the Cu-Al-Ni alloy, as noted above.

In the previous discussion we have neglected the change in ν as a function of $\mathbf{q}$. If this is taken into account, the intensity distribution along each streak is given according to Eq. [5′]. As is well known,[24,25] ν changes sinusoidally with $\mathbf{q}$ to a first approximation, although details differ for each material. Thus, the streak intensities are strong in the vicinity of the reciprocal lattice point. This tendency is clearly seen in all diffraction patterns of Figs. 1 and 2.

The above analysis will be good enough to support the notion that $\langle 110\rangle^*_\beta$ rel rods originate from a transverse acoustic $\langle 110\rangle^*\langle\bar{1}10\rangle$ phonon mode. In fact, this result is consistent with the theoretical predictions by Komatsu and Teramoto for bcc crystals, as briefly discussed in Ref. 26.

We now turn to the diffuse patterns. It was established above that $\langle 110\rangle^*_\beta$ rel rods are present which join fundamental reflections, and that along lines joining superlattice reflections the rods are negligibly weak. Thus, we consider the former rel rods and neglect the latter. Then, the intersections of these streaks with the Ewald sphere give rise to diffuse patterns. This idea fits surprisingly well with all the complex diffuse patterns in Figs. 1 and 2, as shown by the associated index diagrams.

In the $[\bar{1}10]_\beta$ orientation (Figs. 1 and 2(*j*)), the $[\bar{1}10]^*_\beta$ rel rods are perpendicular to the Ewald sphere. Thus the diffuse reflections in this orientation give a cross section of the $[\bar{1}10]^*_\beta$ rel rods which is elliptic, with a major axis along $[001]^*_\beta$ and a minor axis along $[110]^*_\beta$. Various shapes of diffuse reflections in other orientations were found to be consistent with the intersection of such elliptic rel rods with the Ewald sphere.

Thus far, we have discussed the $\langle 110\rangle^*_\beta$ rel rods with specific reference to Cu-Al-Ni and Cu-Zn alloys, but the analysis is not limited to these alloys. The same principle should apply to other β-phase alloys where the structure is bcc, disregarding ordering, and where the elastic constant C', which represents the resistance to a $\langle 110\rangle^*\langle\bar{1}10\rangle_\beta$ shear, is usually quite soft.[6]

IV. DISCUSSION

In the preceding section $\langle 110\rangle^*$ rel rods in β-phase alloys were analyzed as phonon scattering described by a linear combination of dynamic displacement waves of the form given by Eq. [1], and it was then concluded that the presence of the rel rods originates from low frequency transverse acoustic $\langle 110\rangle^*\langle\bar{1}10\rangle$ phonon modes. From a purely theoretical diffraction point of view, however, the same $\langle 110\rangle^*$ rel rods can also be accounted for by other static displacement waves in general. We examine such a possibility in the following. First we consider a static displacement wave of the form

$$\mathbf{R}'_n = A'\boldsymbol{\epsilon}_0 \cos 2\pi\mathbf{q}\cdot\mathbf{r}_n \qquad [1']$$

where $\mathbf{q} \parallel \langle 110\rangle^*$ and $\boldsymbol{\epsilon}_0 \parallel \langle\bar{1}10\rangle$. Using an argument similar to the one presented in Section 3, the $\langle 110\rangle^*$ rel rods can be accounted for by taking a linear combination of the above displacement waves and adopting a model such that the dynamic displacement waves given in the previous section have been "quenched". According to such a model, atoms must sit in unstable positions in the β-phase in a static manner, which is quite unlikely.

As a second static displacement model we can consider stacking faults, microtwins, or anitphase do-

main boundaries. If any of these is the origin of ⟨110⟩* rel rods, then the fault plane, twin plane, jor plane of the antiphase boundary must be a {110} plane and striations along {110} should be observed. Such were never seen. Furthermore it is to be pointed out that neither faulting nor twinning are possible on the {110} plane of β-phase alloys. This is because there are only two possible stacking sites, A and B, and no other sites for faulting on the {110} plane, and the {110} plane is a mirror plane, which precludes twinning. This leaves only the possibility of {110} antiphase domain boundaries to consider. But no such boundaries

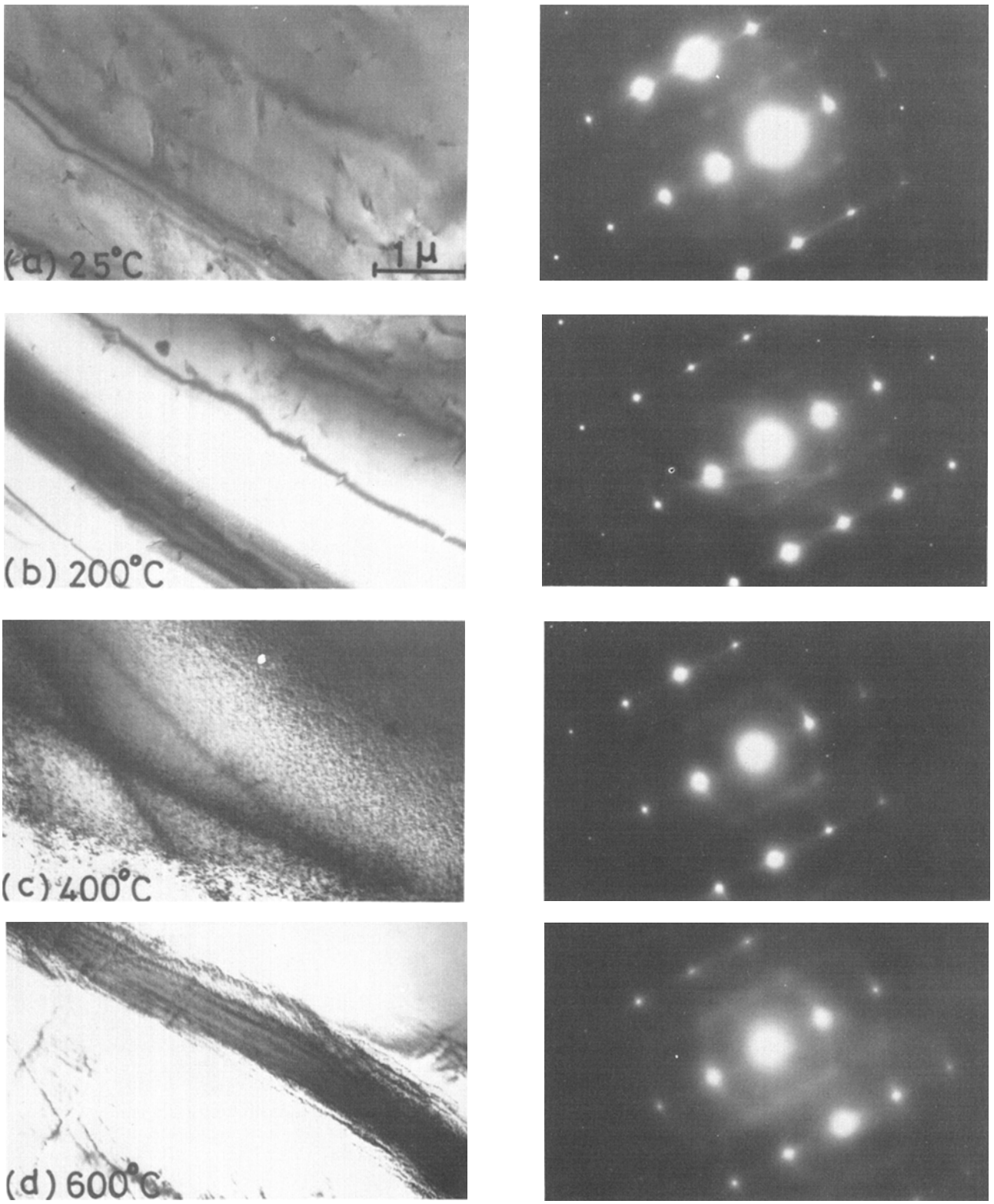

Fig. 3—Variation of diffuse streak patterns upon heating the Cu-Al-Ni alloy from room temperature to 600 C. $[\bar{1}13]_\beta$ orientation.

were detected by dark field imaging using superlattice reflections, and this possibility is ruled out.

The above reasoning supports the conclusion that the $\langle 110\rangle^*$ rel rods originate from dynamic rather than static displacements.

The next question concerns the relation between $\langle 110\rangle^*$ rel rods and $\{\bar{1}11\}^*_\beta$ rel walls. Honjo *et al*[16] suggested that the rel walls were produced by linear chain motions where rows of atoms in the close-packed directions move, more or less, as a rigid body, independently of each other. Later, Komatsu and Teramoto[26] related the linear chain motion with low frequency transverse acoustic waves. However, a direct correlation between the two is not obvious from their paper. If their assertion holds, both $\langle 110\rangle^*_\beta$ rel rods and $\{\bar{1}11\}^*_\beta$ rel walls in the β-phase alloys evidently stem from the same origin, and one asks why there are two different phenomena from one "source". This question was not addressed. We also note the assumption that the chain direction is parallel to the polarization vector of the low frequency acoustic wave. This cannot be the case in β-phase alloys, because the chain direction would have to be $\langle 111\rangle_\beta$, while the polarization vector lies along $\langle 110\rangle_\beta$. Furthermore, rel walls are observed even in aluminum,[16] in which the anisotropy factor is close to unity and in which the $\langle 110\rangle^*\langle\bar{1}10\rangle$ acoustic wave is not very soft relative to those in other branches, *e.g.*, $\langle 100\rangle^*\langle 010\rangle$. Thus it is unlikely that there would be a one-to-one correspondence between low frequency transverse acoustic waves in one branch and rel walls in one direction. In fact when the frequencies of transverse acoustic waves are substantially low, we expect that the atoms in planes normal to the wave vector move as a whole, instead of an independent linear chain motion in each plane. Thus we expect the presence of rel rods rather than rel walls in such a case. We conclude that what is directly correlated with low frequency transverse acoustic waves is not rel walls, but rather rel rods in the direction of the phonon wave vector.

The temperature dependence of the rel rods is of particular interest with respect to "pretransformation" phenomena. Thus this effect was examined by heating several Cu-Al-Ni specimens inside the electron microscope. As shown in Fig. 3, however, there was little observed change upon heating to 600°C, other than the tendency for the rel rods to gradually smear out into $\{111\}^*$ rel planes with increasing temperature. It is to be emphasized that quantitative intensity information is difficult to obtain by electron diffraction, especially when a heating stage is employed, because the Bragg condition varies during heating.

The smearing of rel rods into rel planes might possibly be interpreted as follows. At higher temperatures the atoms move rather randomly along the close-packed directions, but with decreasing temperature this random motion tends to become more correlated in each $\{110\}_\beta$ plane to produce a $\langle 110\rangle^*\langle\bar{1}10\rangle$ shear wave prior to the onset of the martensitic transformation at a lower temperature. It may be only coincidental, but nevertheless it is worth noting that the above $\{110\}_\beta$ plane and $\langle\bar{1}10\rangle_\beta$ direction corresponds to the phenomenological shear movements required in the lattice deformation from a β-matrix to a martensitic phase with a long period stacking order structure (*i.e.*, $2H$, $9R$, $18R$). In this description the lattice correspondence is such that the (close-packed) basal plane of the martensite is parallel to the above mentioned $\{110\}_\beta$ plane, and the $\langle\bar{1}10\rangle_\beta$ displacement is the very direction required for the shuffling to generate an elementary unit cell of martensite with a long period stacking order structure. Thus, the $\langle 110\rangle^*_\beta$ rel rods and a martensitic transformation may be correlated in this manner, but no direct evidence on this point has been obtained as yet.

ACKNOWLEDGMENTS

The authors are grateful to Professors K. Shimizu, Osaka University, K. Teramoto, Osaka Prefecture University, and T. Suzuki, Yokahama City University, for helpful discussions. This work was supported by the National Science Foundation through the Materials Research Laboratory at the University of Illinois.

REFERENCES

1. L. Kaufman and M. Cohen: *Progr. Met. Phys.*, 1958, vol. 7, p. 165.
2. P. C. Clapp: *Phys. Status Solidi B*, 1973, vol. 57, p. 561.
3. T. Suzuki and M. Wuttig: *Acta Met.*, 1975, vol. 23, p. 1069.
4. G. B. Olson and M. Cohen: *Met. Trans. A*, 1976, vol. 1A, p. 1897.
5. S. Mahajan, M. L. Green, and D. Brasen: *Met. Trans. A*, 1977, vol. 8A, p. 283.
6. N. Nakanishi: in *Shape Memory Effects in Alloys*, J. Perkins, ed., p. 147, Plenum Press, New York, 1975.
7. M. Suezawa and K. Sumino: *Scr. Met.*, 1976, vol. 10, p. 789.
8. C. Zener: *Phys. Rev.*, 1947, vol. 71, p. 846.
9. H. Morikawa, K. Shimizu, and Z. Nishiyama: *Trans. Jap. Inst. Metals*, 1967, vol. 8, p. 145.
10. L. Delaey, J. Perkins, and T. B. Massalski: *J. Mater. Sci.*, 1972, vol. 7, p. 1197.
11. W. Vandermeulen and A. Deruyttere: *Met. Trans.*, 1973, vol. 4, p. 1659.
12. T. Takezawa and H. Sato: *J. Jap. Inst. Metals* (in Japanese), 1973, vol. 37, p. 793.
13. Z. Nishiyama, K. Shimizu, and H. Morikawa: *Jap. J. Appl. Phys.*, 1967, vol. 6, p. 815.
14. L. Delaey and H. Warlimont: in *Shape Memory Effects in Alloys*, J. Perkins, ed., p. 89, Plenum Press, New York, 1975.
15. A. Nagasawa: *J. Phys. Soc. Jap.*, 1976, vol. 40, p. 93.
16. G. Honjo, S. Kodera, and N. Kitamura: *J. Phys. Soc. Jap.*, 1964, vol. 19, p. 351.
17. K. Enami, J. Hasunuma, A. Nagasawa, and S. Nenno: *Scr. Met.*, 1976, vol. 10, p. 879.
18. K. Otsuka and C. M. Wayman: *Phys. Status Solidi*, 1967, vol. 22, p. 579.
19. K. Chandra and G. R. Purdy: *J. Appl. Phys.*, 1968, vol. 39, p. 2176.
20. G. D. Sandrock, A. J. Perkins, and R. F. Hehemann: *Met. Trans.*, 1971, vol. 2, p. 2769.
21. S. Vatanayon and R. F. Hehemann: in *Shape Memory Effects in Alloys*, J. Perkins, ed., p. 115, Plenum Press, New York, 1975.
22. A. Guinier: *X-ray Diffraction in Crystals, Imperfect Crystals and Amorphous Bodies*, W. H. Freeman and Co., San Francisco, 1963.
23. S. Hoshino, G. Shirane, M. Suezawa, and T. Kajitani: *Jap. J. Apply. Phys.*, 1975, vol. 14, p. 1233.
24. S. C. Moss and C. M. Wayman: Unpublished research, University of Houston, 1976.
25. C. Kittel: *Introduction to Solid State Phys.*, 4th ed., John Wiley and Sons, Inc., New York, 1971.
26. K. Komatsu and K. Teramoto: *J. Phys. Soc. Jap.*, 1966, vol. 21, p. 1152.